

Galactic Rotation Curve and the Effect of Density Waves from Data on Young Objects

V.V. Bobylev, A.T. Bajkova, and A.S. Stepanishchev,

Central (Pulkovo) Astronomical Observatory of RAS, St-Petersburg

Abstract—Based on currently available data on the three-dimensional field of space velocities of young (≤ 50 Myr) open star clusters and the radial velocities of HI clouds and star-forming (HII) regions, we have found the Galactic rotation curve in the range of Galactocentric distances $3 \text{ kpc} < R < 12 \text{ kpc}$ using the first six terms of the Taylor expansion of the angular velocity of Galactic rotation in Bottlinger's equations. The Taylor terms found at the Galactocentric distance of the Sun $R_0 = 7.5 \text{ kpc}$ are: $\omega_0 = -27.7 \pm 0.6 \text{ km s}^{-1} \text{ kpc}^{-1}$, $\omega_0^1 = 4.13 \pm 0.07 \text{ km s}^{-1} \text{ kpc}^{-2}$, $\omega_0^2 = -0.912 \pm 0.065 \text{ km s}^{-1} \text{ kpc}^{-3}$, $\omega_0^3 = 0.277 \pm 0.036 \text{ km s}^{-1} \text{ kpc}^{-4}$, $\omega_0^4 = -0.265 \pm 0.034 \text{ km s}^{-1} \text{ kpc}^{-5}$, $\omega_0^5 = 0.104 \pm 0.020 \text{ km s}^{-1} \text{ kpc}^{-6}$. In this case, the Oort constants are $A = 15.5 \pm 0.3 \text{ km s}^{-1} \text{ kpc}^{-1}$ and $B = -12.2 \pm 0.7 \text{ km s}^{-1} \text{ kpc}^{-1}$. We have established that the centroid of the sample moves relative to the local standard of rest along the Galactic Y axis with a velocity of $-6.2 \pm 0.8 \text{ km s}^{-1}$. A Fourier spectral analysis of the velocity residuals from the derived rotation curve attributable to density waves reveals three dominant peaks with wavelengths of 2.5, 1.4, and 0.9 kpc and amplitudes of 4.7, 2.6, and 3.6 km s^{-1} , respectively. These have allowed us to estimate the distances between the density wave peaks, 1.9, 2.4, and 3.2 kpc as R increases, in agreement with the description of the density wave as a logarithmic spiral. The amplitude of the density wave perturbations is largest in the inner part of the Galaxy, $\approx 9 \text{ km s}^{-1}$, and decreases to $\approx 1 \text{ km s}^{-1}$ in its outer part. A spectral analysis of the radial velocities of young open star clusters has confirmed the presence of periodic perturbations with an amplitude of $5.9 \pm 1.1 \text{ km s}^{-1}$ and a wavelength $\lambda = 1.7 \pm 0.5 \text{ kpc}$. It shows that the phase of the Sun in the density wave is close to $-\pi/2$ and the Sun is located in the interarm space near the outer edge of the Carina-Sagittarius arm.

INTRODUCTION

Constructing the Galactic rotation curve is of great importance in solving a number of problems, such as estimating the mass of the Galaxy, determining the distribution of matter, estimating the hidden mass, studying the dynamics of the Galaxy and its subsystems, etc. The shape of the rotation curve in the outer Galaxy is of particular interest. Xue et al. (2008) showed that the circular rotation velocity is close to 200 km s^{-1} far from the Galactic center, being 175 km s^{-1} at a distance of 60 kpc.

The following data on various objects in the Galactic disk are used to determine the Galactic rotation parameters: HI and HII radial velocities (Burton 1971; Clemens 1985; Fich et al. 1989; Brand and Blitz 1993; Nikiforov 1999; Russeil 2003; Avedisova 2005), data on open star clusters (OSCs) and associations, Cepheids and other young stars (Mishurov and Zenina 1999; Rastorguev et al. 1999; Dambis et al. 2001; Zabolotskikh et al. 2002; Dias and Lépine 2005).

The most comprehensive information about the pattern of Galactic rotation in the inner region can be obtained using the radial velocities of hydrogen clouds extracted from 21-cm or CO radio observations.

Once the theory of spiral density waves has been developed (Lin and Shu 1964; Lin et al. 1969), it turned out that the small deviations of the circular velocities of hydrogen clouds from the smooth rotation curve constructed from radial velocities could be successfully interpreted in terms of the density wave theory (Burton 1971; Burton and Gordon 1978; Clemens 1985). However, the hydrogen radial velocity data are insufficient to trace the kinematic effect of the spiral pattern in the outer Galaxy. (Indeed, since the tangential point method is inapplicable, the hydrogen data have large errors.) Therefore, other data, for example, those on OSCs, should be invoked additionally.

When only the radial velocities are analyzed, the following two quantities serve as model ones for constructing the Galactic rotation curve: the Galactocentric distance of the Sun R_0 and the linear circular velocity of the Sun V_0 (Brand and Blitz 1993; Russeil 2003; Avedisova 2005). Including OSCs for which reliable estimates of their proper motions are available allows us either to reduce the number of model quantities to one (R_0), because in this case the angular velocity of solar rotation ω_0 can be determined from observations (Rastorguev et al. 1999; Zabolotskikh et al. 2002), or to determine both R_0 and V_0 directly from observational data (Bobylev et al. 2007).

The goal of this paper is to solve two problems: (1) constructing a smooth rotation curve from young objects in the Galactic disk and (2) analyzing the high-frequency periodic circular velocity residuals of the objects used from the derived rotation curve attributable to the effect of spiral density waves.

To solve the first problem, the R range is usually broken down into several segments: the central ($R < 0.8 - 1.5R_0$), inner ($\approx 1.5R_0 < R < R_0$), and outer ($R > R_0$) regions of the Galaxy, as was done by Burton (1971) and Clemens (1985). This approach is used mainly because there is a segment of solid-body rotation in the inner Galaxy that passes into a fairly flat curve further out. Therefore, the entire R range is difficult to describe by a smooth curve. In addition, there are significant radial motions of gas at $R < 3$ kpc (Bania 1977; Liszt and Burton 1980). Several authors suggested their smoothed rotation curves for each of these regions (Burton and Gordon 1978; Clemens 1985). However, it is not always convenient to use a rotation curve defined by different expressions in different R segments. It is much more convenient to have one analytical expression for the rotation curve in the entire range.

Here, we restrict our analysis to the range of distances $R > 2.5$ kpc. Zabolotskikh et al. (2002) found a smoothed Galactic rotation curve in a wide range of distances R without dividing it into segments, but this rotation curve was given in tabular form, which complicates its use. Our objective is to determine the Galactic rotation curve in a wide range of distances, $R > 2.5$ kpc, in analytical form.

We use a Fourier spectral analysis to analyze the velocity residuals of the objects from

the derived rotation curve produced by a spiral density wave.

Apart from the radial velocities of hydrogen clouds, we invoke data on star-forming regions (Russeil 2003) and new data on young OSCs (Kharchenko et al. 2007). To determine the projections of the OSC circular velocities, we use their total space velocities.

DATA

The Working Data Set

We took the radial velocities of HI clouds obtained by the tangential point method from Fich et al. (1989), where the 21-cm hydrogen radio observations described in Burton and Gordon (1978) are presented in tabular form. We also used the CO radio observations by the tangential point method from Clemens (1985).

We took the data on star-forming (H II) regions mainly from the catalog by Russeil (2003), which contains the radial velocities and photometric distances for 204 regions. In this paper, we use only 89 HII regions selected according to the following criteria:

- (i) the relative random errors in the distances to the objects do not exceed 20%;
- (ii) the regions are located outside the zone with the Galactic center–anticenter direction $|l| < 12^\circ$, where the chance of estimating the radial velocities is reduced sharply (Russeil 2003);
- (iii) the regions have Galactocentric distances of more than 5 kpc (closer regions are rejected because of the large velocity dispersion).

For the HII region Sharpless 294, we use a new estimate of its photometric distance, $r = 4.8 \pm 0.2$ kpc, from Samal et al. (2007). For the star-forming region W3OH, we use a new estimate of its distance, $r = 1.95 \pm 0.04$ kpc, from Xu et al. (2006) obtained from the trigonometric parallax (0.512 ± 0.010 mas) measured using the VLBA. For the HII region Sharpless 269, we use the results of high-precision radio interferometry (Honma et al. 2007): the trigonometric parallax 0.189 ± 0.008 mas ($r = 5.28 \pm 0.23$ kpc), the radial velocity $V_{LSR} = 19.6$ km s⁻¹, and the proper motion components $(\mu_\alpha \cos \delta, \mu_\delta)_{J2000} = (-0.422 \pm 0.010, -0.121 \pm 0.042)$ mas determined relative to an extragalactic source. Thus, these data allow the space velocities of the region Sharpless 269 to be determined.

For OSCs, we use the coordinates, proper motions, radial velocities, and age estimates from the compilation by Bobylev et al. (2007), which is based on the catalog by Piskunov et al. (2006). We took new radial velocities for a number of OSCs from the CRVOCA catalog (Kharchenko et al. 2007). In this paper, we consider only the OSCs whose ages do not exceed 50 Myr and for which the space velocities can be determined. We took the data for two young clusters, Cr 272 and Tr 28, which are missing from the CRVOCA catalog, from the catalog by Dias et al. (2002).

Heliocentric Radial Velocities

We will work with the radial velocity estimates for the objects given in the heliocentric frame of reference. Different authors give their radial velocity estimates relative to the local standard of rest using differing parameters — $(U, V, W)_{LSR}$.

We reduce the hydrogen radial velocities from Burton and Gordon (1978) and Clemens (1985) to the heliocentric frame of reference using the velocities $(U, V, W)_{LSR} =$

(10.3, 15.3, 7.7) km s⁻¹. We calculated these values based on the following parameters of the standard solar motion: $(\alpha, \delta)_{1900} = (270^\circ, +30^\circ)$ and $V = 20$ km s⁻¹ (Burton and Gordon 1978).

We reduce the radial velocities of the star-forming regions to the heliocentric frame of references using the velocities $(U, V, W)_{LSR} = (10.4, 14.8, 7.3)$ km s⁻¹ from Russeil (2003).

We reduce the radial velocities of the HII region Sharpless 269 to the heliocentric frame of reference using the velocities $(U, V, W)_{LSR} = (10.0, 15.4, 7.8)$ km s⁻¹ from Honma et al. (2007).

All proper motions of the objects are given for the epoch J2000.0, i.e., they are homogeneous. Therefore, no problem with their reduction to a single frame of reference arises.

METHODS

In this paper, we use a rectangular Galactic coordinate system with the axes directed away from the observer toward the Galactic center ($l = 0^\circ, b = 0^\circ$, the X axis), along the Galactic rotation ($l = 90^\circ, b = 0^\circ$, the Y axis), and toward the North Galactic Pole ($b = 90^\circ$, the Z axis).

Determining the Rotation-Curve Parameters

The method used here is based on Bottlinger's well-known formulas (Ogorodnikov 1958) with the angular velocity of Galactic rotation expanded in a series to terms of the sixth order of smallness in r/R_0 :

$$\begin{aligned} V_r = & -u_\odot \cos b \cos l - & (1) \\ & -v_\odot \cos b \sin l - w_\odot \sin b - \\ & -R_0 \sin l \cos b [(R - R_0)\omega_0^1/1! + \\ & + \dots + (R - R_0)^5 \omega_0^5/5!], \end{aligned}$$

$$\begin{aligned} V_l = & u_\odot \sin l - v_\odot \cos l - & (2) \\ & -(R_0 \cos l - r \cos b) [(R - R_0)\omega_0^1/1! + \\ & + \dots + (R - R_0)^5 \omega_0^5/5!] + \\ & + r\omega_0 \cos b, \end{aligned}$$

$$\begin{aligned} V_b = & u_\odot \cos l \sin b + & (3) \\ & + v_\odot \sin l \sin b - w_\odot \cos b + \\ & + R_0 \sin l \sin b [(R - R_0)\omega_0^1/1! + \\ & + \dots + (R - R_0)^5 \omega_0^5/5!], \end{aligned}$$

where V_r is the radial velocity; $V_l = 4.74r\mu_l \cos b$ and $V_b = 4.74r\mu_b$ are the proper motion velocity components in the l and b directions, respectively (the coefficient 4.74 is the quotient of the number of kilometers in the astronomical unit by the number of seconds in the tropical year); r is the heliocentric distance of the object; the proper motion components $\mu_l \cos b$ and μ_b are in mas yr⁻¹, the radial velocity V_r is in km s⁻¹; $u_\odot, v_\odot, w_\odot$ are the solar velocity components relative to the centroid under consideration; R_0 is the Galactocentric distance of the Sun, which we take to be $R_0 = 7.5$ kpc (Bobylev et al. 2007); R is the Galactocentric

distance of the object; R , R_0 , and r are in kpc. The quantity ω_0 is the angular velocity of rotation at the distance R_0 , the parameters $\omega_0^1, \dots, \omega_0^5$ are the derivatives of the angular velocity from the first to the fifth order, respectively. The distance R can be calculated using the expression

$$R^2 = r^2 \cos^2 b - 2R_0 r \cos b \cos l + R_0^2. \quad (4)$$

Note also that Eqs. (1)–(3) are written in such a way that the direction of rotation from the X axis to the Y axis is positive. The system of conditional equations (1)–(3) contains nine unknowns: $u_\odot, v_\odot, w_\odot$, $\omega_0, \omega_0^1, \omega_0^2, \omega_0^3, \omega_0^4, \omega_0^5$, which can be determined by the least-squares method. Equations (1)–(3) can be easily generalized to determine any necessary number of terms of the series in the expansion of the angular velocity of rotation ω_0^n . The system of equations (1)–(3) is solved with weights of the form

$$P_{(r,l,b)} = S_0 / \sqrt{S_0^2 + \sigma_{V_{r,l,b}}^2},$$

where P_r is the weight of the equation for the radial velocity, P_l and P_b are the corresponding weights for the components V_l and V_b , and S_0 denotes the dispersion averaged over all observations, which has the meaning of the “cosmic” dispersion that we take to be 8 km s^{-1} . The errors σ_{V_l} and σ_{V_b} in the velocities V_l and V_b can be calculated using the formulas

$$\sigma_{(V_l, V_b)} = 4.74r \sqrt{\mu_{l,b}^2 \left(\frac{\sigma_r}{r}\right)^2 + \sigma_{\mu_{l,b}}^2},$$

where σ_π/π is taken to be 0.2, a typical error in the photometric distance for OSCs.

Determining the Projections V_{rot} and V_{rad}

When only the radial velocity is available for an object, we calculate the projection of the circular rotation velocity V_{rot} from the well-known formula (Burton 1971)

$$V_{rot} = |R\omega_0| + RV_r / (R_0 \sin l \cos b). \quad (5)$$

For OSCs, we have the rectangular coordinates X, Y, Z and calculate the components of the observed space velocities U and V from the projections V_r, Vl , and V_b (Kulikovskii 1985). Using these components, we find two projections, V_{rad} directed radially away from the Galactic center and V_{rot} orthogonal to it, from the relations

$$V_{rot} = U \sin \theta + (V_0 + V) \cos \theta, \quad (6)$$

$$V_{rad} = -U \cos \theta + (V_0 + V) \sin \theta, \quad (7)$$

where $V_0 = |R_0\omega_0|$ and the position angle θ is defined as $\tan \theta = Y/(R_0 - X)$. We assume that the velocities U and V are free from the solar velocity relative to the centroid $V_\odot(u_\odot, v_\odot, w_\odot)$ derived above from Eqs. (1)–(3). The errors in the projections V_{rad} and V_{rot} can be estimated from the relations

$$\sigma^2(V_{rot}) = \sigma_U^2 \sin^2 \theta + \sigma_V^2 \cos^2 \theta,$$

$$\sigma^2(V_{rad}) = \sigma_U^2 \cos^2 \theta + \sigma_V^2 \sin^2 \theta,$$

where the errors in the space velocities U and V are denoted by σ_U and σ_V .

Analysis of the Residual Velocities

At the next step, we consider the rotation velocities ΔV that are the residual ones with respect to the Galactic rotation curve found at the first step.

A spectral analysis consists in applying the direct Fourier transform to the sequence of residual velocities in the following way:

$$\overline{\Delta V}(\lambda_k) = \frac{1}{M} \sum_i^M \Delta V^i \exp\left(-j \frac{2\pi}{\lambda_k} R_i\right), \quad (8)$$

where $\overline{\Delta V}(\lambda_k)$ is the value of harmonic k of the Fourier transform, M is the number of measurements of the residual velocities ΔV^i with coordinates R_i , $i = 1, 2, \dots, M$, and λ_k is the wavelength in kpc; the latter is equal to D/k , where D is the period of the original sequence in kpc.

Constraints

The constraints listed below reduce significantly the error of a unit weight when the system of equations (1)–(3) is solved by the least-squares method.

For HII regions: (i) the error in the distance is no more than 20%; (ii) $R > 5$ kpc; (iii) location outside the zone with the Galactic center-anticenter direction $|l| < 12^\circ$.

For OSCs: (i) the age is younger than 50 Myr; (ii) the error in the modulus of the space velocity is $\sqrt{\sigma_{R_V}^2 + \sigma_{V_i}^2 + \sigma_{V_b}^2} < 15$ km s⁻¹; (iii) $V_{pec} = \sqrt{U^2 + V^2 + W^2} < 100$ km s⁻¹. In particular, we also use condition (i), because the negative K-effect, i.e., the effect of radial motions (Bobylev et al. 2007), for young OSCs is less pronounced than that for older ones.

For neutral hydrogen (HI): (i) $R > 2.4$ kpc; (ii) several radial velocities from Burton and Gordon (1978) are not used; these data are marked by the circles in Figs. 3a and 4. At the same time, when analyzing the residual velocities, we rejected only two points close to the Sun. Condition (i) is used, because a transition to the zone of solid-body rotation is observed on the rotation curve at $R \approx 2.4$ kpc (Burton 1971; Clemens 1985).

The system of conditional equations (1)–(3) is solved twice with an analysis of the residuals using the 3σ criterion (we clearly see from Fig. 4 that the points rejected by this criterion have large residuals).

RESULTS

At a fixed Galactocentric distance of the Sun ($R_0 = 7.5$ kpc), by solving the system of 777 equations, we found the parameters of the solar velocity relative to the centroid, $(u_\odot, v_\odot, w_\odot) = (8.41, 11.41, 8.01) \pm (0.49, 0.50, 0.64)$ km s⁻¹, and the parameters of the angular velocity of Galactic rotation,

$$\begin{aligned} \omega_0 &= -27.67 \pm 0.61 \text{ km s}^{-1} \text{ kpc}^{-1}, \\ \omega_0^1 &= +4.132 \pm 0.072 \text{ km s}^{-1} \text{ kpc}^{-2}, \\ \omega_0^2 &= -0.912 \pm 0.065 \text{ km s}^{-1} \text{ kpc}^{-3}, \\ \omega_0^3 &= +0.277 \pm 0.036 \text{ km s}^{-1} \text{ kpc}^{-4}, \end{aligned} \quad (9)$$

$$\begin{aligned}\omega_0^4 &= -0.265 \pm 0.034 \text{ km s}^{-1} \text{ kpc}^{-5}, \\ \omega_0^5 &= +0.104 \pm 0.020 \text{ km s}^{-1} \text{ kpc}^{-6}.\end{aligned}$$

As a result, taking into account all constraints, we used the data for 140 young OSCs (including S269) with a mean age of 18 Myr, 89 radial velocities of the HII regions (Russeil 2003), 135 radial velocities for the tangential points (CO) from Clemens (1985), and 133 radial velocities for the tangential points (H I) from Burton and Gordon (1978). The error of a unit weight is $\sigma_0 = 8.0 \text{ km s}^{-1}$.

As a result, the Oort constants $A = 0.5R_0\omega_0^1$, $B = \omega_0 + 0.5R_0\omega_0^1$, are $A = 15.50 \pm 0.27 \text{ km s}^{-1} \text{ kpc}^{-1}$ and $B = -12.17 \pm 0.67 \text{ km s}^{-1} \text{ kpc}^{-1}$.

Based on parameters (9), we estimated the circular rotation velocity of the solar neighborhood to be $V_0 = |R_0\omega_0| = 208 \pm 5 \text{ km s}^{-1}$ and the period of its revolution around the Galactic center to be $T = 2\pi/(\gamma \omega_0) = 221 \text{ Myr}$, where the coefficient $\gamma = 1.023 \times 10^{-9} [\text{km s}^{-1} \text{ kpc}^{-1}]/[\text{rad yr}^{-1}]$ (Murray 1986).

Figure 1 shows the coordinates of the objects being analyzed in projection onto the Galactic XY plane.

Figure 2 shows the Galactic rotation curve constructed from parameters (9); the OSC circular velocity projections were calculated only from radial velocities using Eq. (5). As can be seen from Eq. (5), the division by $\sin l$ is made in the second term. Hence, the projections of the objects with l close to zero have large deviations and large errors. In Fig. 2, the open squares mark 17 OSCs with $|l| < 12^\circ$. Therefore, Eq. (5) is not used to analyze the OSC velocities.

Figures 3a and 3b show the OSC circular velocity projections calculated using Eq. (6). The thick solid line in these figures indicates the derived rotation curve. Figures 3a and 3b differ by the age of the OSCs used, whose velocities are denoted by the circles. Figure 3a pertains to young OSCs (younger than 50 Myr), while Fig. 3b pertains to old OSCs (older than 50 Myr). We see from the figure that the velocities of both young and old OSCs fall nicely on the derived Galactic rotation curve; in contrast to the old OSCs, the young OSCs exhibit a distinct high-frequency component related to the effect of density waves. The dotted line in Fig. 3a indicates the Galactic rotation curve from Zabolotskikh et al. (2002), which was found using seven terms in the expansion of the angular velocity. From the figure, we see good agreement between the two rotation curves for $R > 3.5 \text{ kpc}$.

We solved Eqs. (1)–(3) using various numbers of terms in the expansion of ω_0 . A direct construction of the rotation curves shows that adding each succeeding term extends significantly the boundaries of the confidence interval. However, it can be said with confidence that three expansion terms are clearly not enough to construct the Galactic rotation curve in the range of distances $3 \text{ kpc} < R < 12 \text{ kpc}$ (Bobylev et al. 2007), while seven terms are too many. For example, when the seventh term is added to Eqs. (1)–(3), terms that do not differ significantly from zero appear: $\omega_0^3 = +0.107 \pm 0.086 \text{ km s}^{-1} \text{ kpc}^{-4}$ and $\omega_0^6 = -0.076 \pm 0.035 \text{ km s}^{-1} \text{ kpc}^{-7}$, with the shape of the curve remaining virtually unchanged. In this sense, we found an optimal solution.

We can see from our comparison of the OSC circular velocities in Figs. 2 and 3a that the projections calculated using Eq. (6) have a smaller residual velocity dispersion with respect to the derived rotation curve.

The dotted line in Fig. 3b denotes the rotation curve as derived by Dias and Lépine (2005) for $R_0 = 7.5 \text{ kpc}$; we added a constant term of 18 km s^{-1} to $V_0 = 190 \text{ km s}^{-1}$ to

reconcile it with our data at $R = R_0(V_0 = 208 \text{ km s}^{-1})$.

Figure 4 shows the angular velocity of Galactic rotation determined using parameters (9). The circles mark the HI data points rejected by the 3σ criterion when seeking for the rotation curve. Note, however, that these points were not rejected at the second step during our spectral analysis of the high-frequency deviations. Based on Fig. 4, we choose the range of distances $3 \text{ kpc} < R < 12 \text{ kpc}$ as the most significant one.

The R distribution of the residual velocities obtained by subtracting the derived Galactic rotation curve from the original distribution of circular velocities is shown in Fig. 5. This distribution corresponds to the case where no OSCs are used, i.e., here we essentially repeated the analysis by Clemens (1985). The result obtained is discussed in the next section. Figure 5b corresponds to the entire set of objects under consideration. The residual velocity dispersion is 8.8 km s^{-1} . The maximum residual velocity is 45 km s^{-1} . As we see from the figure, a periodic structure of the velocity distribution attributable to the effect of Galactic spiral density waves is traceable. Therefore, it is quite natural to use a spectral analysis to investigate the residual velocities in an effort to obtain quantitative characteristics.

We can see from our comparison of Figs. 5a and 5b that the fitting residual velocity curve in Fig. 5b has more distinct peaks; the similarity of the two periods in the inner Galaxy is better seen in this curve than in the curve of Fig. 5a.

Figure 6 shows the power spectra of the residual velocities as a function of the natural logarithm of the wavelength-to- R_0 ratio ($\ln \lambda/R_0$). Figure 6a pertains to the residual velocities ΔV_I obtained by subtracting $V_{rot} - V_0$ (where we found the velocity $V_0 = 208 \text{ km s}^{-1}$ above), representing the deviation from a flat rotation curve, while Fig. 6b pertains to the residual velocities ΔV_{II} obtained by subtracting the derived Galactic rotation curve from the original distribution of V_{rot} (Fig. 5b).

The power spectra are fairly wide, but we give them only up to $\ln \lambda/R_0 = -3.5$. The amplitude of the spectrum decreases rapidly with increasing frequency (decreasing wavelength).

We can see from our comparison of Figs. 6a and 6b that taking into account the derived Galactic rotation curve with parameters (9) allows us to get rid of the low-frequency spectral component almost completely.

Three dominant peaks with wavelengths of 2.5, 1.4, and 0.9 kpc ($\ln \lambda/R_0 \approx -1.2, -1.8, -2.2$) and amplitudes of 4.7, 2.6, and 3.6 km s^{-1} , respectively, can be distinguished in the power spectrum of the residual velocities shown in Fig. 6b. The thick line in Fig. 5b indicates the fitting curve of the residuals constructed using the frequencies of the spectrum in Fig. 6b for $\ln \lambda/R_0 > -2.5$. In contrast to the approach by Clemens (1985), who estimated the perturbation wavelength and amplitude only from one dominant peak in the residual power spectrum, we construct the fitting curve in a wider frequency range. As a result, we obtain a complex periodic curve that represents satisfactorily the residuals.

Four main peaks with the following characteristics can be distinguished in Fig. 5b:

- (1) $R_1 = 3.9 \text{ kpc}$, $\Delta V_1 = 8.2 \text{ km s}^{-1}$;
- (2) $R_2 = 5.8 \text{ kpc}$, $\Delta V_2 = 9.2 \text{ km s}^{-1}$;
- (3) $R_3 = 8.2 \text{ kpc}$, $\Delta V_3 = 1.0 \text{ km s}^{-1}$;
- (4) $R_4 = 11.4 \text{ kpc}$, $\Delta V_4 = 1.8 \text{ km s}^{-1}$.

The distance differences between the peaks are $\Delta R_{21} = 1.9 \text{ kpc}$, $\Delta R_{32} = 2.4 \text{ kpc}$ and $\Delta R_{43} = 3.2 \text{ kpc}$. As can be seen from Fig. 5b, the fourth peak is revealed with the lowest confidence. In general, Fig. 5b gives only a qualitative picture of the effect of spiral density waves. This is because the line of sight passes through different sections of the spiral arms

and, hence, the resulting velocity distribution is “smeared”. Nevertheless, we can suggest the following identification with known spiral arms: peak 1 — the Scutum-Crux arm; peak 2 — the Carina-Sagittarius arm; peak 3 — the Perseus arm; peak 4 — the Norma-Cygnus arm. In general, the locations of the first three peaks agree well with the two-arm model by Yuan (1969). Comparison with Figs. 4 and 5 from Russeil (2003) shows that this identification agrees satisfactorily with both three-arm and four-arm models of the spiral pattern (see also Fig. 2 from Vallée (2002)). However, for the best agreement with models, for example, the model by Russeil (2003), we must assume that the peak with $R = 2.9$ kpc and $\Delta V = 1.9$ km s⁻¹ is significant in our Fig. 5b. In this case, it will be either the beginning of the Perseus arm for the three-arm model or the beginning of the Norma-Cygnus arm for the four-arm model.

Figure 7 shows the residual radial velocities of young OSCs as a function of the Galactocentric distance calculated using Eq. (7). The power spectrum of the residual radial velocities for young OSCs obtained using Eq. (8), where the radial velocities are considered as ΔV , is shown in Fig. 8. The curve of residuals shown in Fig. 7 has a wavelength $\lambda = 1.7$ kpc and an amplitude of 5.9 km s⁻¹; the linear displacement along the vertical axis is -1.6 km s⁻¹. We clearly see from our comparison of Figs. 6b and 8 that, in contrast to the circular residual velocities, the power spectrum of the residual radial velocities of young OSCs for wavelengths $\ln \lambda/R_0 > -2.5$ is simpler: in fact, there is only one distinct and symmetric peak near $\ln \lambda/R_0 \approx -1.7$. Therefore, the derived curve of residuals is nearly sinusoidal in the range $R = 6.9$ kpc.

When the circular velocities are analyzed, the error in λ is ± 0.3 kpc and the error in the perturbation velocity amplitude is ± 0.5 km s⁻¹ (504 points). We estimated these values by the Monte Carlo method. When the radial velocities of 140 young OSCs are analyzed, these errors have the following values: the error in λ is ± 0.5 kpc and the error in the perturbation velocity amplitude is ± 1.1 km s⁻¹.

DISCUSSION

The Galactic Rotation Curve

Having analyzed the data on hydrogen clouds in a wide R range, up to $2R_0$, Brand and Blitz (1993) found a nearly flat Galactic rotation curve ($A = -B$). However, the Oort constants $A = 15.50 \pm 0.27$ km s⁻¹ kpc⁻¹ and $B = -12.17 \pm 0.67$ km s⁻¹ kpc⁻¹ we found, which are in good agreement with the result of various recent studies (for an overview of the determinations of the Oort constants, see Bobylev 2004), show that the rotation curve in the solar neighborhood is nevertheless not flat. The low-frequency peak in Fig. 6a shows that the amplitude of the deviations of the Galactic rotation curve from a flat one is about 8 km s⁻¹ in the range $3 \text{ kpc} < R < 12 \text{ kpc}$.

Note that, in general, our Galactic rotation curve in the R range under consideration agrees satisfactorily with the “composite” rotation curve by Clemens (1985).

The shape of the rotation curve in the outer Galaxy depends significantly on the adopted value of R_0 (Clemens 1985; Olling and Merrifield 2000; Zabolotskikh et al. 2002). Our Galactic rotation curve is intermediate between the two rotation curves from Olling and Merrifield (2000) constructed using currently available data for $R_0 = 7.1$ and 8.5 kpc.

As we see from Fig. 3a, our Galactic rotation curve agrees well, within the 1σ confidence interval, with one of the best (since it was constructed by carefully reconciling the distance scales of various samples) curves to date constructed by Zabolotskikh et al. (2002) for $R_0 = 7.5$ kpc.

As we see from Fig. 3b, our Galactic rotation curve differs significantly from the rotation curve that was found by Dias and Lépine (2005) using data from Clemens (1985) only in the distant outer part of the Galaxy ($R > 11$ kpc). This difference stems from the fact that the observational data in the outer Galaxy are scarce, while the available data are unreliable. In this respect, the unique observational data for S269 (Fig. 3a) are of great importance.

In general, it can be concluded that our Galactic rotation curve in the range $3 \text{ kpc} < R < 12 \text{ kpc}$ under consideration describes well the observational data used and is in good agreement with the results of other authors.

The Phase of the Sun in the Spiral Wave

Having analyzed the velocities of HI clouds in the inner Galaxy, Clemens (1985) found the deviation of the motion of the local standard of rest from the circular one with a velocity $\Delta V_{rot} = +7.0 \pm 1.5 \text{ km s}^{-1}$ in the direction of Galactic rotation.

In our view, this motion can also be associated with the effect of a density wave. Let us consider an example from Rohlfs (1977),

$$\begin{aligned}\sigma_1 &= |\hat{\sigma}| \cos \chi, \\ V_{rad} &= -|f_R| \cos \chi, \\ \Delta V_{rot} &= |f_\theta| \sin \chi\end{aligned}\tag{10}$$

for the region within the corotation radius in the case of a tightly wound spiral. Here, $\chi = f(R, \chi_\odot)$ is the phase of the spiral wave, χ_\odot is the phase of the Sun in the spiral wave, σ_1 is the matter density, $\hat{\sigma}$ is the density perturbation amplitude, f_R and f_θ are the amplitudes of the radial and tangential velocity perturbation components, the center of the spiral arm corresponds to the phase $\chi = 0$ (for details, see the description to Fig. 21 in the monograph by Rohlfs (1977)). For the case of $\Delta V_{rot} = +7.0 \text{ km s}^{-1}$ under consideration, the phase of the solar neighborhood in the wave will be close to $-\pi/2$. It thus follows that the Sun is located at the outer edge of the arm.

The solar velocity components $V_\odot(u_\odot, v_\odot, w_\odot)$ we found lead us to conclude that there is a motion of the centroid of our sample along the Galactic Y axis with a velocity $\Delta V_{rot} = V_{LSR} - v_\odot = -6.2 \pm 0.8 \text{ km s}^{-1}$ relative to the local standard of rest with parameters $(U, V, W)_{LSR} = (10.00, 5.25, 7.17) \pm (0.36, 0.62, 0.38) \text{ km s}^{-1}$ (Dehnen and Binney 1998) that differs significantly from zero. Note that Dehnen and Binney (1998) determined the velocity of the Sun relative to the local standard of rest based on the proper motions of ≈ 12000 main-sequence stars from the Hipparcos Catalogue (1997). Our previous analysis (Bobylyev and Bajkova 2007) of the space velocities for ≈ 5000 F and G dwarfs using radial velocities showed that $(U, V, W)_{LSR} = (8.7, 6.2, 7.2) \pm (0.5, 2.2, 0.8) \text{ km s}^{-1}$. Thus, the reliability of the parameters $(U, V, W)_{LSR}$ is beyond doubt.

As we see, the velocity ΔV_{rot} of the centroid of our sample along the Y axis is negative. Hence, in this case, the Sun should be located at the inner edge of the spiral arm, having a phase close to $\pi/2$. This contradiction between the two estimates of the phase of the Sun was also pointed out by Zabolotskikh et al. (2002).

It is clearly seen from Fig. 5a, where we essentially repeated the analysis of data from Clemens (1985), that the perturbation velocity in the solar neighborhood is positive, $\Delta V_{rot} = +2 \text{ km s}^{-1}$. As can be seen from Fig. 5b, including the data on OSCs in the analysis changes significantly the picture in the immediate neighborhood of the Sun. The perturbation velocity at $R = R_0$ is $\Delta V_{rot} = -5.5 \pm 0.5 \text{ km s}^{-1}$; the phase of the Sun in the wave should then be close to $\pi/2$.

However, we again run into a significant contradiction. If the phase of the Sun is assumed to be close to $\pi/2$, then the radial velocities should decrease with increasing distance from the Sun in the direction of increasing R , but the reverse is true in Fig. 7.

Note that our OSC residual velocity distributions (Figs. 5b and 7) are in good agreement with the results of the analyses of the velocity (V_R and V_θ) fields for OB associations performed by several authors: see Fig. 3 in Mel'nik et al. (2001) and Fig. 1 in Mel'nik (2003).

We associate the above contradictions with the influence of the Orion arm, since a significant fraction of the nearby OSCs (Fig. 1) belong to this structure. In the opinion of several authors (Yuan 1969; Weaver 1970; Elmegreen 1980; Efremov 1997), the Orion arm is a branch at the outer edge of the Cygnus spiral arm (Melnik 2003) or a spur. Previously, Bobylev et al. (2007) found that the centroid of the OSCs belonging to the Orion arm lags behind the local standard of rest with a velocity of $\approx -10 \text{ km s}^{-1}$, while the typical lag velocity for the centroids of the OSC belonging to other arms is $\approx -5 \text{ km s}^{-1}$.

All of the data obtained are difficult to reconcile within the framework of a simple model. As was shown by Sitnik and Mel'nik (1999) and Mel'nik (2003, 2006), the real picture of the solar neighborhood may be much more complex.

Nevertheless, the phase of the Sun in the spiral wave can be determined from radial velocities. The amplitude of the OSC radial velocity perturbations is higher than that of the circular velocity perturbations. The radial velocities are almost free from the discrepancy in the velocities of the centroid and the local standard of rest (see the vertical displacement in Fig. 7). The amplitude of the radial velocity perturbations is essentially determined by the spiral density wave. Thus, for example, as was pointed out by Lin et al. (1969), the stars in the solar neighborhood can go away from their birthplace to distances of $\sim 1.2 \text{ kpc}$ over a period of $\sim 10 \text{ Myr}$, which is attributable mainly to the rotation velocities, while the stars go away in the radial direction to distances that are a factor of 10 smaller due to the small pitch angle of the spiral arms. Based on the data in Fig. 7, we conclude that the phase of the Sun in the density wave is slightly larger than $-\pi/2$ (a more accurate value is $\chi_\odot = -0.66\pi$). Consequently, the Sun is located in the interarm space near the outer edge of the Carina-Sagittarius arm. This location of the Sun agrees well with the distribution of stars and gas (Vallée 2002; Russeil 2003) and with predictions of the density-wave theory. Indeed, as we see from relations (10), the variations in velocity V_{rad} are in phase with the variations in density σ_1 .

The Scale Factor λ

The distance between the neighboring spiral arms along the Galactic radius vector is usually denoted by λ ; occasionally, it is called a scale factor or scale length (Mel'nik et al. 2001).

Clemens (1985) obtained an estimate of $\lambda = 0.22R_0$. For the value of $R_0 = 8.5 \text{ kpc}$ used by him, this gives $\lambda = 1.9 \text{ kpc}$, which is in good agreement with our results.

Having analyzed the space velocities of OB associations within 3 kpc of the Sun, Mel'nik et al. (2001) estimated the scale length of the periodic variations in radial residual velocity components along the Galactic radius vector to be $\lambda = 2.0 \pm 0.2$ kpc.

At the same time, we found that the distance between the spiral arms does not remain constant in the R range under consideration and is $\Delta R_i = 1.9, 2.4, 3.2$ kpc. This is in agreement with the description of the density wave as a logarithmic spiral, as distinct from an Archimedean spiral characterized by a constant distance between the neighboring turns of the spiral. Details of the discussion on the specific shape of the spiral in the Galaxy can be found in the monograph by Efremov (1989). The model using an Archimedean spiral was suggested by Cowie and Rybicki (1982).

Having analyzed the radial velocities of young OSCs, we obtained an independent estimate of $\lambda = 1.7 \pm 0.5$ kpc from data in the range of distances $6 \text{ kpc} < R < 9 \text{ kpc}$.

The Perturbation Amplitudes

The perturbation amplitudes of the circular, $f_\theta = 4.6 \pm 0.5 \text{ km s}^{-1}$ (the main peak in Fig. 6b), and radial, $f_R = 5.9 \pm 1.1 \text{ km s}^{-1}$ (the main peak in Fig. 8), velocities that we found are in good agreement with the minimum perturbation amplitude of 5 km s^{-1} (at the minimum wavelength $\lambda = 0.22R_0$) estimated by Clemens (1985).

Based on formulas from Lin et al. (1969), Burton (1971) estimated the change in the amplitudes of the perturbation velocities from a density wave (f_R and f_θ) as a function of R in the range $0.2R_0 < R < 1.3R_0$. It turned out that for both velocities, there is a wide peak in the region $0.5R_0 < R < 0.9R_0$, where the velocities reach $\approx 8 \text{ km s}^{-1}$ (f_R is larger than f_θ by $\approx 1 \text{ km s}^{-1}$ everywhere), the velocities are about 4 km s^{-1} near $0.2R_0$ and decrease to 2.5 km s^{-1} near $1.3R_0$. Our results (Fig. 5b) agree well with the estimates by Burton (1971).

However, it is hard to say that our results are in good agreement with those of other authors obtained for the solar neighborhood. Thus, for example, having analyzed OB associations, Mel'nik et al. (2001) found the velocities of the perturbations from a spiral density wave to be $f_R = 7 \pm 1 \text{ km s}^{-1}$ and $f_\theta = 2 \pm 1 \text{ km s}^{-1}$. Popova and Loktin (2005) obtained completely different velocities of the perturbations from a spiral density wave, $f_R = -4 \pm 5 \text{ km s}^{-1}$ and $f_\theta = 13 \pm 3 \text{ km s}^{-1}$, using data on OSCs and OB stars. Based on Cepheids, Mishurov and Zenina (1999) found $f_R = 3.3 \pm 1.6 \text{ km s}^{-1}$ and $f_\theta = -7.9 \pm 2.0 \text{ km s}^{-1}$. The analysis of data on Cepheids performed by Popova (2006) showed that the amplitude of the perturbation velocities, $f_R = -1.8 \pm 2.5 \text{ km s}^{-1}$ and $f_\theta = 4.0 \pm 3.4 \text{ km s}^{-1}$ are small and do not differ significantly from zero. Zabolotskikh et al. (2002) found $f_R \approx -7 \pm 2 \text{ km s}^{-1}$ and $f_\theta \approx -1 \pm 2 \text{ km s}^{-1}$ from data on Cepheids and OSCs.

In general, our results lead us to conclude that the curve in Fig. 5b describes well the large-scale (grand design) spiral structure; there are peculiarities at $R = R_0$ attributable to the kinematic properties of the Orion arm.

CONCLUSIONS

Based on currently available data on the three-dimensional field of space velocities of young ($\leq 50 \text{ Myr}$) open star clusters and the radial velocities of HI clouds and star-forming (H II)

regions, we constructed the Galactic rotation curve in the range of Galactocentric distances $3 \text{ kpc} < R < 12 \text{ kpc}$.

At the first step, we determined a smoothed curve that fitted fairly accurately the Galactic rotation curve in this range of distances. The curve parameters (9) were found by using the first six terms of the Taylor expansion of the angular velocity of Galactic rotation at a given Galactocentric distance of the Sun, $R_0 = 7.5 \text{ kpc}$. We found that the centroid of the sample moves relative to the local standard of rest along the Galactic Y axis with a velocity of $-6.2 \pm 0.8 \text{ km s}^{-1}$.

At the second step, we performed a spectral analysis of the circular velocity residuals of the objects under consideration from the derived rotation curve, which attributes the observed periodic residuals to the effect of density waves. Our spectral analysis showed that the peak with an amplitude of $4.6 \pm 0.5 \text{ km s}^{-1}$ corresponding to a wavelength $\lambda = 2.5 \pm 0.3 \text{ kpc}$ is dominant. A similar analysis of the radial velocities for young OSCs confirmed the presence of periodic perturbations from a density wave with an amplitude of $5.9 \pm 1.1 \text{ km s}^{-1}$ and a wavelength $\lambda = 1.7 \pm 0.5 \text{ kpc}$.

Based on the described approach, Clemens (1985) obtained similar results, but only for the inner Galaxy ($R < R_0$), where highly accurate data on hydrogen are available for tangential points. In contrast, for the outer Galaxy ($R > R_0$), the radial velocities of hydrogen (HI and HII) clouds usually have large errors, which makes it much more difficult to interpret the residuals.

We were able to advance slightly farther than R_0 , because we used the total space velocities of OSCs to determine the projections of their circular velocities. In our view, this approach improves the homogeneity of the sample. The tangential point method allows the total space velocity of hydrogen clouds to be analyzed, since the velocity vector lies entirely on the line of sight under the assumption of purely circular rotation of hydrogen at the tangential point. Therefore, supplementing the sample of objects with OSCs seems natural.

We found that the distance between the spiral arms increases with Galactocentric distance, being 1.9, 2.4, and 3.2 kpc; this is in agreement with the description of the density wave as a logarithmic spiral. The perturbation amplitude also changes — it is largest in the inner part of the Galaxy, $\approx 9 \text{ km s}^{-1}$, and decreases to $\approx 1 \text{ km s}^{-1}$ in its outer part.

Analysis of the radial velocities of a sample of young OSCs suggests that the phase of the Sun in the density wave is close to $-\pi/2$ and that the Sun is located in the interarm space near the outer edge of the Carina-Sagittarius arm.

ACKNOWLEDGMENTS

We wish to thank R.-D. Scholz, who provided the version of the CRVOCA catalog even before its appearance in the Strasbourg database, S.V. Lebedeva for help in working with our database, and the referees for useful remarks that contributed to an improvement of the paper. This work was supported by the Russian Foundation for Basic Research (project no. 08-02-00400).

REFERENCES

1. V. S. Avedisova, *Astron. Zh.* 82, 488 (2005) [*Astron. Rep.* 49, 435 (2005)].

2. T. M. Bania, *Astroph. J.* 216, 381 (1977).
3. V. V. Bobylev, *Pis'ma Astron. Zh.* 30, 185 (2004) [*Astron. Lett.* 30, 159 (2004)].
4. V. V. Bobylev, A. T. Bajkova, and S. V. Lebedeva, *Pis'ma Astron. Zh.* 33, 809 (2007) [*Astron. Lett.* 33, 720 (2007)].
5. V. V. Bobylev and A. T. Bajkova, *Astron. Zh.* 84, 418 (2007) [*Astron. Rep.* 51, 372 (2007)].
6. J. Brand and L. Blitz, *Astron. Astrophys.* 275, 67 (1993).
7. W. B. Burton, *Astron. Astrophys.* 10, 76 (1971).
8. W. B. Burton and M. A. Gordon, *Astron. Astrophys.* 63, 7 (1978).
9. L. L. Cowie and G. B. Rybicki, *Astroph. J.* 260, 504 (1982).
10. D. P. Clemens, *Astroph. J.* 295, 422 (1985).
11. A. K. Dambis, A. M. Mel'nik, and A. S. Rastorguev, *Pis'ma Astron. Zh.* 27, 68 (2001) [*Astron. Lett.* 27, 58 (2001)].
12. W. Dehnen and J. J. Binney, *Mon. Not. R. Astron. Soc.* 298, 387 (1998).
13. W. S. Dias, B. S. Alessi, A. Moitinho, et al., *Astron. Astrophys.* 389, 971 (2002).
14. W. S. Dias and J. R. D. Lépine, *Astroph. J.* 629, 825 (2005).
15. Yu. N. Efremov, *Sites of Star Formation in Galaxies* (Nauka, Moscow, 1989) [in Russian].
16. Yu. N. Efremov, *Pis'ma Astron. Zh.* 23, 659 (1997) [*Astron. Lett.* 23, 579 (1997)].
17. D. M. Elmegreen, *Astroph. J.* 242, 528 (1980).
18. M. Fich, L. Blitz, and A. A. Stark, *Astroph. J.* 342, 272 (1989).
19. *The Hipparcos and Tycho Catalogues*, ESA SP-1200 (1997).
20. M. Honma, T. Bushimata, Y. K. Choi, et al., *astroph/0709.0820v1* (2007).
21. N. V. Kharchenko, R.-D. Scholz, A. E. Piskunov, et al., *Astron. Nachr.* 328 (2007).
22. P. G. Kulikovskii, *Stellar Astronomy* (Nauka, Moscow, 1985) [in Russian].
23. H. S. Liszt and W. B. Burton, *Astroph. J.* 236, 779 (1980).
24. C. C. Lin and F. H. Shu, *Astroph. J.* 140, 646 (1964).
25. C. C. Lin, C. Yuan, and F. H. Shu, *Astroph. J.* 155, 721 (1969).
26. A. M. Mel'nik, A. K. Dambis, and A. S. Rastorguev, *Pis'ma Astron. Zh.* 27, 521 (2001) [*Astron. Lett.* 27, 521 (2001)].
27. A. M. Mel'nik, *Pis'ma Astron. Zh.* 29, 349 (2003) [*Astron. Lett.* 29, 304 (2003)].
28. A. M. Mel'nik, *Pis'ma Astron. Zh.* 32, 9 (2006) [*Astron. Lett.* 32, 7 (2006)].
29. Yu. N. Mishurov and I. A. Zenina, *Astron. Astrophys.* 341, 81 (1999).
30. C. A. Murray, *Vectorial Astrometry* (Adam Hilger, Bristol, 1983).
31. I. I. Nikiforov, *Astron. Zh.* 76, 403 (1999) [*Astron. Rep.* 43, 345 (1999)].
32. K. F. Ogorodnikov, *Dynamics of Stellar Systems* (Fizmatgiz, Moscow, 1958; Pergamon, Oxford, 1965).
33. R. P. Olling and M. R. Merrifield, *Mon. Not. R. Astron. Soc.* 311, 361 (2000).
34. M. E. Popova and A. V. Loktin, *Pis'ma Astron. Zh.* 31, 743 (2005) [*Astron. Lett.* 31, 663 (2005)].
35. M. E. Popova, *Pis'ma Astron. Zh.* 32, 274 (2006) [*Astron. Lett.* 32, 244 (2006)].
36. A. E. Piskunov, N. V. Kharchenko, S. Röser, et al., *Astron. Astrophys.* 445, 545 (2006).
37. A. S. Rastorguev, E. V. Glushkova, A. K. Dambis, and M. V. Zabolotskikh, *Pis'ma Astron. Zh.* 25, 689 (1999) [*Astron. Lett.* 25, 595 (1999)].
38. K. Rohlfs, *Lectures on Density Wave Theory* (Springer-Verlag, Berlin, 1977; Mir, Moscow, 1980).
39. D. Russeil, *Astron. Astrophys.* 397, 133 (2003).
40. M. R. Samal, A. K. Pandey, D. K. Ojha, et al., *astroph/0708.4137v1* (2007).
41. T. G. Sitnik and A. M. Mel'nik, *Pis'ma Astron. Zh.* 25, 194 (1999) [*Astron. Lett.* 25, 156 (1999)].
42. Y. Xu, M. J. Reid, X. W. Zheng, et al., *Science* 311, 54 (2006).

43. X.-X. Xue, H. W. Rix, G. Zhao, et al., *astro-ph/0801.1232v1* (2008). 44. J. P. Vallée, *Astroph. J.* 566, 261 (2002).
45. H. Weaver, in *Proceedings of the IAU Symposium: Interstellar Gas Dynamics*, Ed. by H. Habing (Reidel, Dordrecht, 1970), Vol. 39, p. 22.
46. C. Yuan, *Astroph. J.* 158, 871 (1969).
47. M. V. Zabolotskikh, A. S. Rastorguev, and A. K. Dambis, *Pis'ma Astron. Zh.* 28, 516 (2002) [*Astron. Lett.* 28, 454 (2002)].

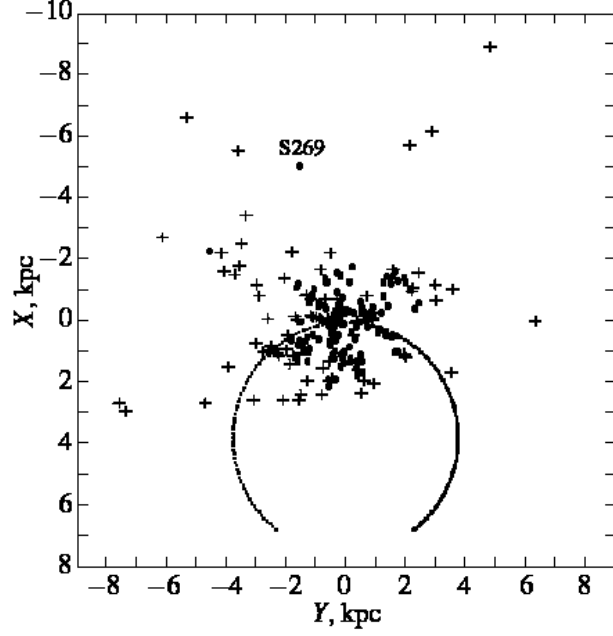


Fig. 1. Coordinates of the objects being analyzed in projection onto the Galactic XY plane. The Sun lies at the coordinate origin. The pluses, dots, and filled circles denote the HII regions, tangential points, and OSCs, respectively.

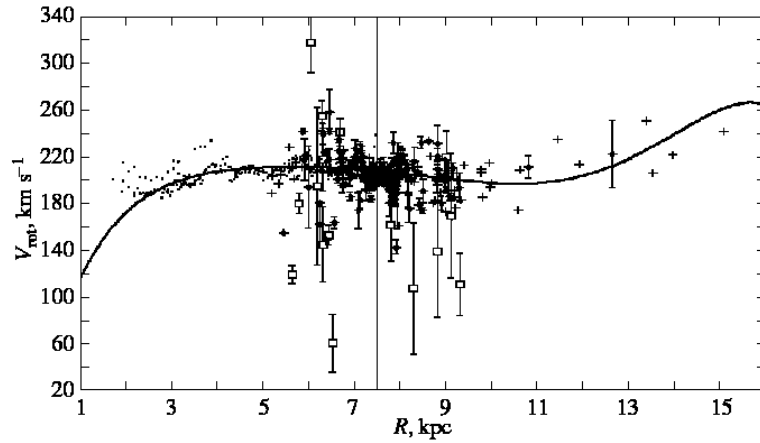


Fig. 2. Galactic rotation curve. The vertical line indicates $R_0 = 7.5$ kpc. For OSCs, the velocities were calculated only from the radial velocities using Eq. (5).

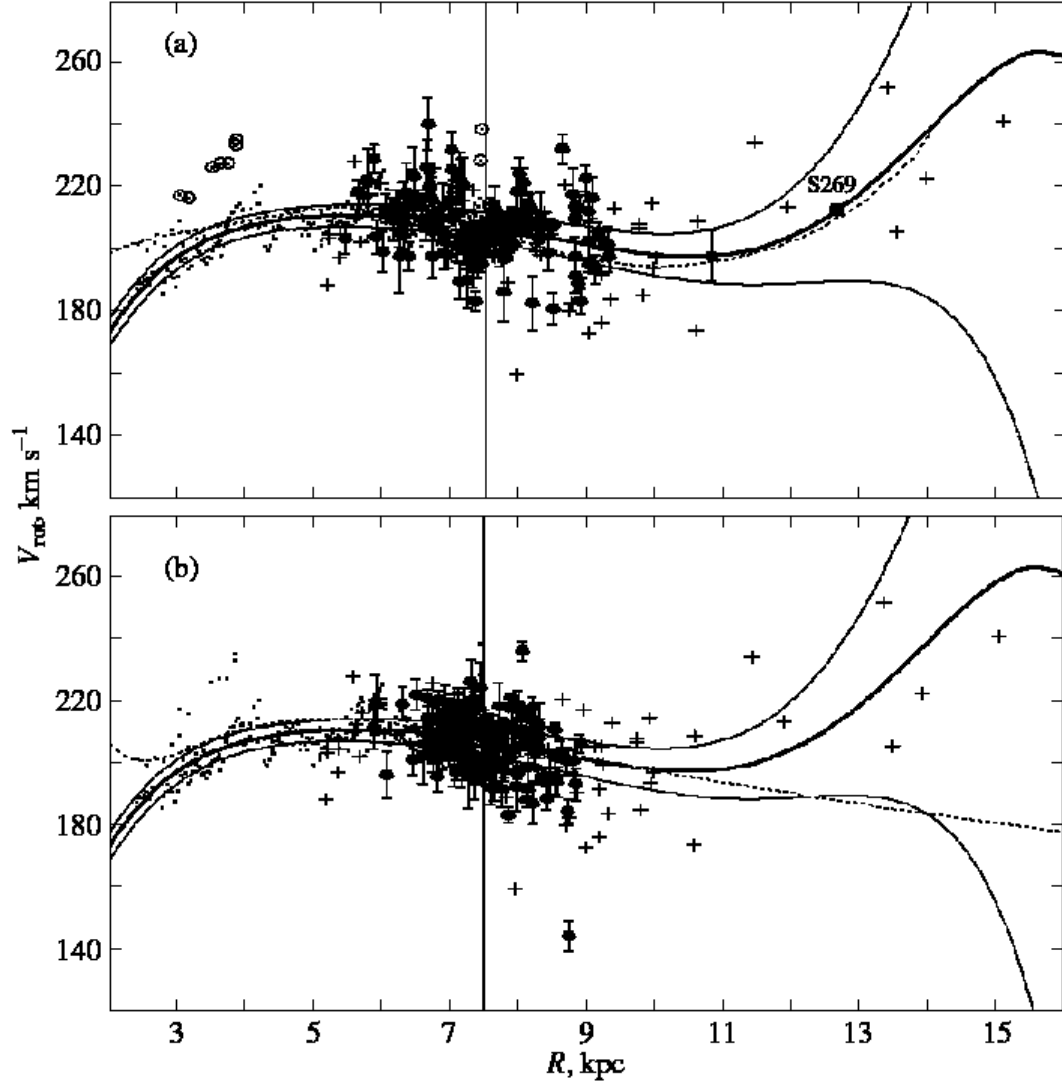


Fig. 3. Galactic rotation curve (thick line), the thin lines mark the boundaries of the 1σ confidence intervals, the vertical line indicates $R_0 = 7.5$ kpc, the symbols \odot in panel (a) mark the tangential points that were not used to determine the rotation curve parameters and the remaining symbols are the same as those in Fig. 1. The dotted line in panels (a) and (b) denote the rotation curve as derived by Zabolotskikh et al. (2002) and Dias and Lépine (2005), respectively.

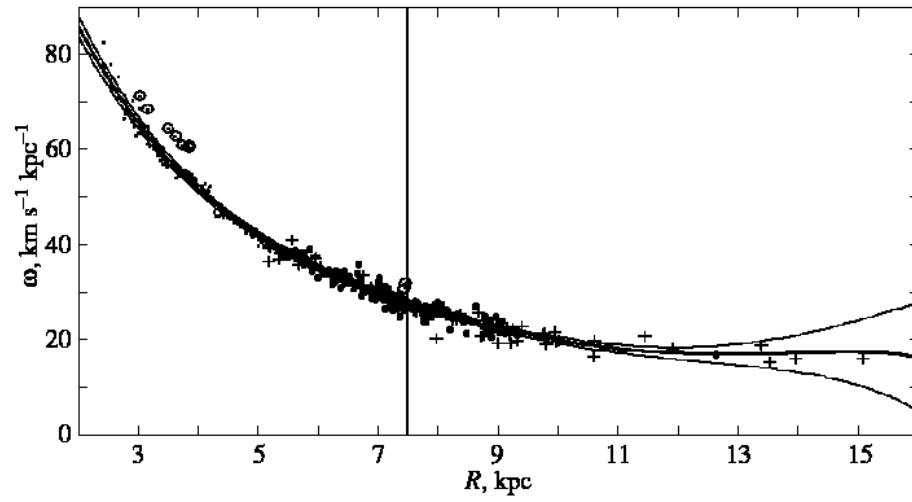


Fig. 4. Angular velocity of Galactic rotation versus Galactocentric distance. The symbols are the same as those in Figs. 1 and 3, the thin lines mark the boundaries of the 1σ confidence intervals, and the vertical line indicates $R_0 = 7.5 \text{ kpc}$.

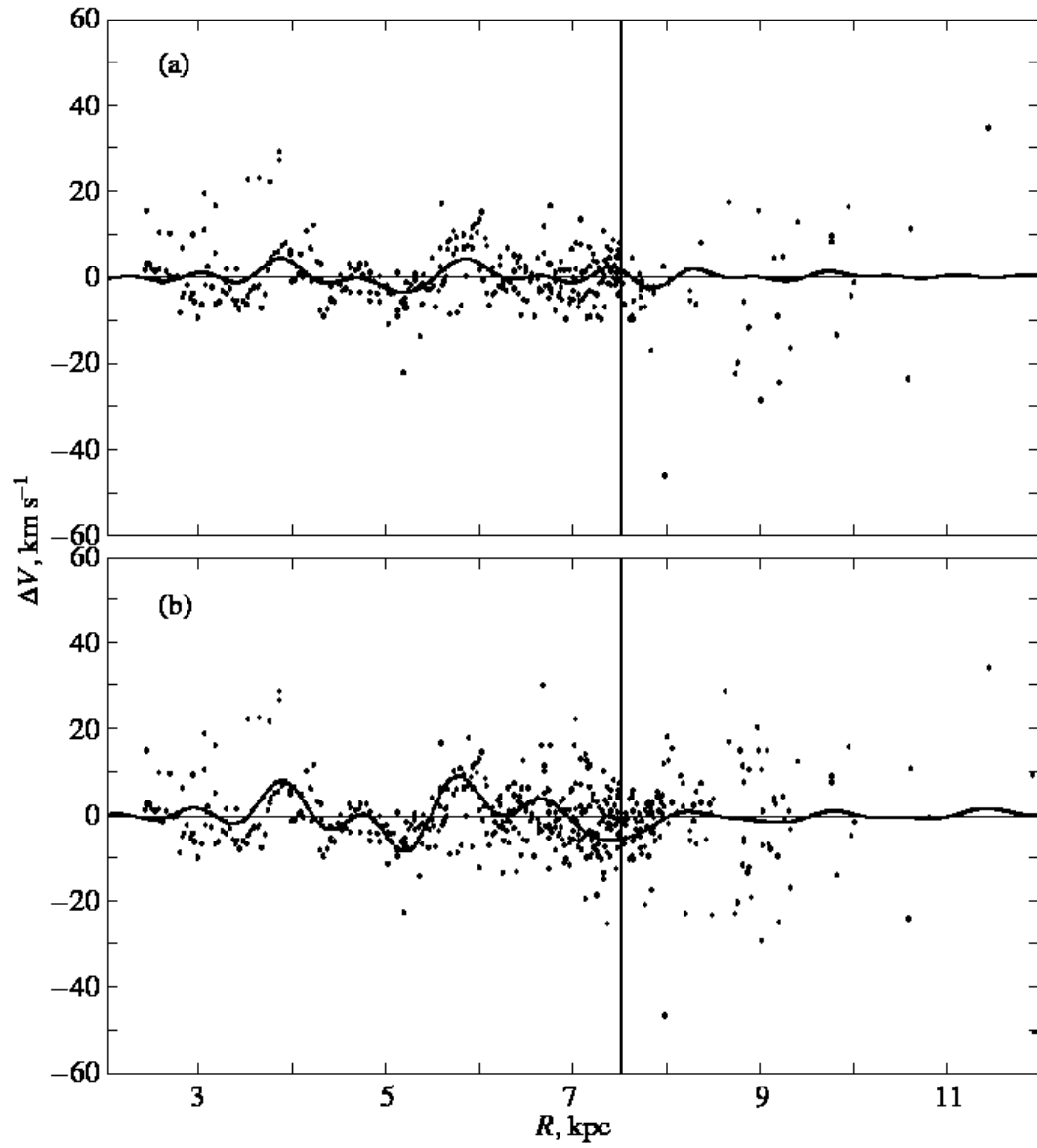


Fig. 5. Residual circular velocities versus Galactocentric distance: (a) no OSCs are used; (b) the entire set of objects being analyzed is used.

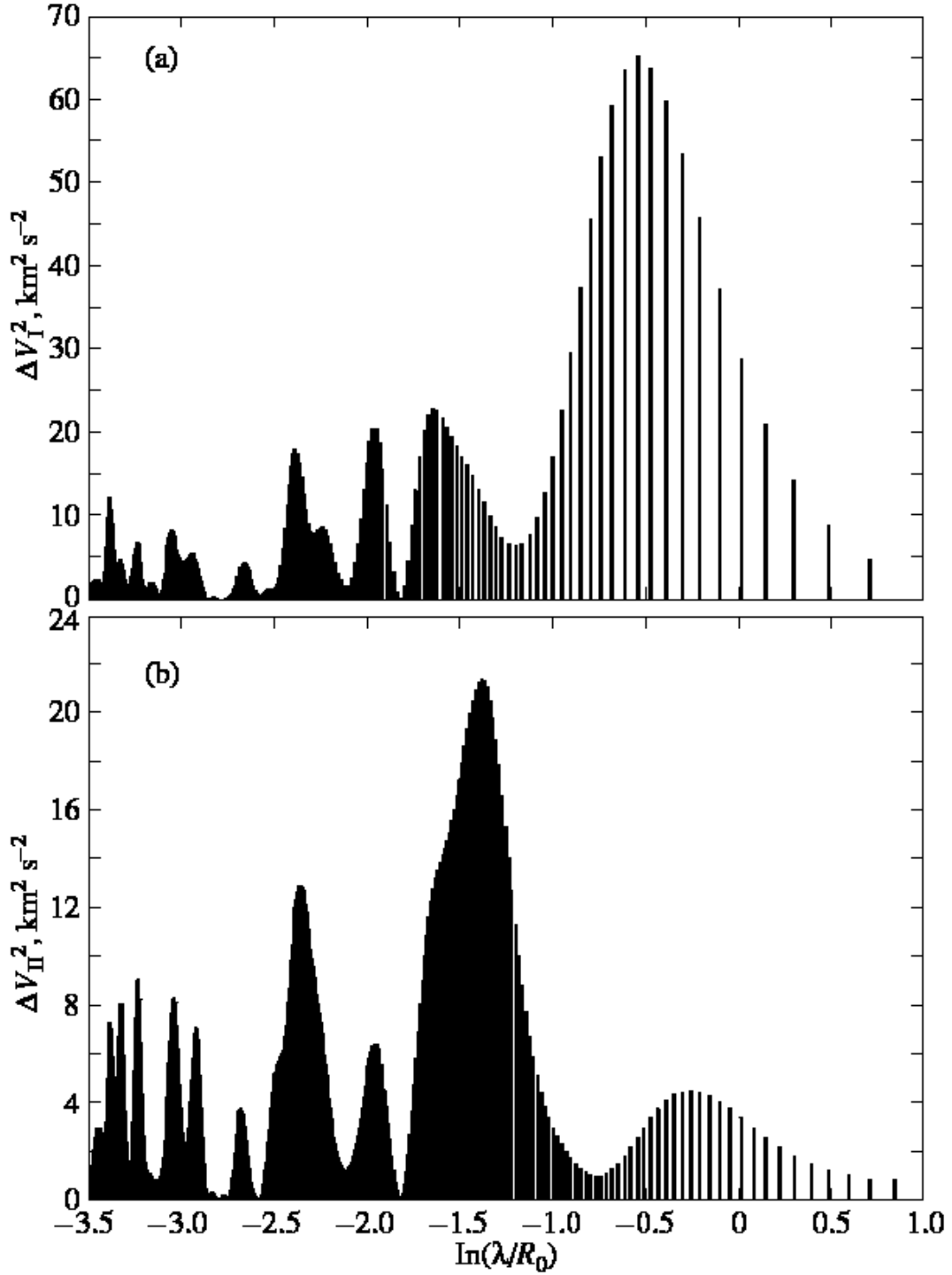


Fig. 6. Power spectrum of the residual rotation velocities as a function of $\ln(\lambda/R_0)$: (a) residual velocities relative to the flat curve; (b) residual velocities relative to curve (9).

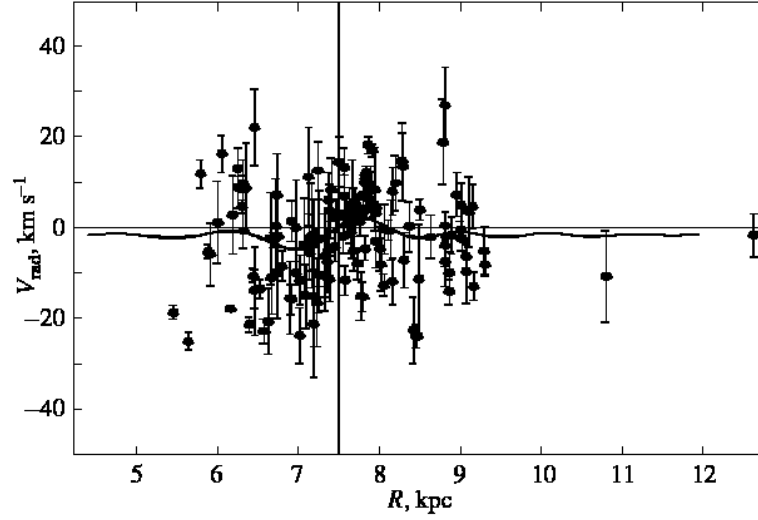


Fig. 7. Residual radial velocities of young OSCs versus Galactocentric distance.

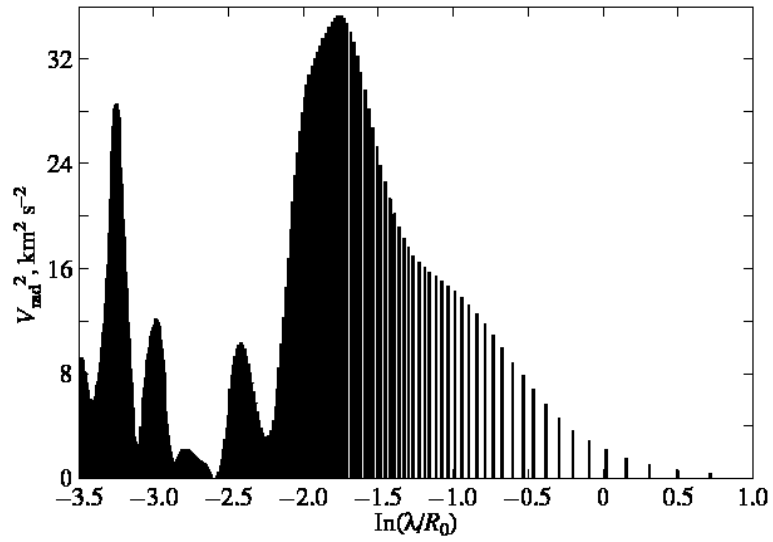


Fig. 8. Power spectrum of the residual radial velocities for young OSCs as a function of $\ln(\lambda/R_0)$.